JOURNAL OF ENZYME INHIBITION AND MEDICINAL CHEMISTRY
2022, VOL. 37, NO. 1, 1375–1388
https://doi.org/10.1080/14756366.2022.2073442

Taylor & Francis
Taylor & Francis Group

RESEARCH PAPER

Design, synthesis, and evaluation of novel *O*-alkyl ferulamide derivatives as multifunctional ligands for treating Alzheimer's disease

Gaofeng Zhu[a]*, Ping Bai[b]*, Keren Wang[c]*, Jing Mi[c], Jing Yang[c], Jiaqi Hu[a], Yujuan Ban[a], Ran Xu[a], Rui Chen[a], Changning Wang[b], Lei Tang[a] and Zhipei Sang[a,c]

[a]State Key Laboratory of Functions and Applications of Medicinal Plants, School of Basic Medical Sciences, Guizhou Provincial Engineering Technology Research Center for Chemical Drug R&D, Guizhou Medical University, Guiyang, China; [b]Department of Radiology, Athinoula A. Martinos Center for Biomedical Imaging, Massachusetts General Hospital, Harvard Medical School, Charlestown, MA, USA; [c]College of Chemistry and Pharmaceutical Engineering, Nanyang Normal University, Nanyang, China

ABSTRACT

Herein, a series of novel *O*-alkyl ferulamide derivatives were designed and synthesised through the multi-target-directed ligands (MTDLs) strategy. The biological activities *in vitro* showed that compounds **5a**, **5d**, **5e**, **5f**, and **5h** indicated significantly selective MAO-B inhibitory potency (IC_{50} = 0.32, 0.56, 0.54, 0.73, and 0.86 μM, respectively) and moderate antioxidant activity. Moreover, compounds **5a**, **5d**, **5e**, **5f**, and **5h** showed potent anti-inflammatory properties, remarkable effects on self-induced $A\beta_{1\text{-}42}$ aggregation, and potent neuroprotective effect on $A\beta_{1\text{-}42}$-induced PC12 cell injury. Furthermore, compounds **5a**, **5d**, **5e**, **5f**, and **5h** presented good blood–brain barrier permeation *in vitro* and drug-like properties. More interesting, the PET/CT images with [^{11}C]**5f** demonstrated that [^{11}C]**5f** could penetrate the BBB with a high brain uptake and exhibited good brain clearance kinetic property. Therefore, compound **5f** would be a promising multi-functional agent for the treatment of AD.

GRAPHICAL ABSTRACT

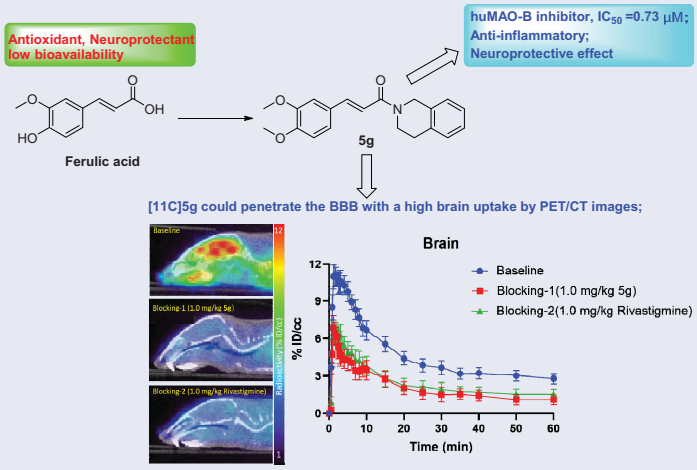

ARTICLE HISTORY
Received 7 January 2022
Revised 5 April 2022
Accepted 28 April 2022

KEYWORDS
Alzheimer's disease; *O*-alkyl ferulamide derivatives; multifunctional agents; PET-CT imaging

1. Introduction

Alzheimer's disease (AD) is first described by Dr. Alois Alzheimer in 1906. It is an irreversible and severe progressive neurodegenerative brain disease[1]. Currently, the approved drugs for treating AD include the *N*-methyl-*D*-aspartate receptor antagonist (memantine) and the cholinesterase inhibitors (rivastigmine, doneipezil, and galantamine), however, these drugs cannot effectively prevent or reverse the progression of AD, but they do provide short-term symptomatic relief[2,3].

The pathogenesis of AD is not clear completely, the characterised pathologic brain changes include amyloid-β (Aβ) deposits, neurofibrillary tangles, and low levels of acetylcholine (ACh). Accumulated evidence shows that over 100 targets relate to AD,

CONTACT Zhipei Sang sangzhipei@126.com State Key Laboratory of Functions and Applications of Medicinal Plants, School of Basic Medical Sciences, Guizhou Provincial Engineering Technology Research Center for Chemical Drug R&D, Guizhou Medical University, Guiyang, 550004, China; Changning Wang cwang15@mgh.harvard.edu Department of Radiology, Athinoula A. Martinos Center for Biomedical Imaging, Massachusetts General Hospital, Harvard Medical School, Charlestown, MA, 02129, USA; Lei Tang tl1974@163.com State Key Laboratory of Functions and Applications of Medicinal Plants, School of Basic Medical Sciences, Guizhou Provincial Engineering Technology Research Center for Chemical Drug R&D, Guizhou Medical University, Guiyang, 550004, China
*These authors contributed equally to this work.

Supplemental data for this article can be accessed here.

and many hypotheses are proposed, such as the cholinergic hypothesis, amyloid cascade hypothesis, tau hypothesis, oxidative stress hypothesis, inflammation hypothesis, metal ion hypothesis, and mutation hypothesis[4].

Monoamine oxidases A and B (MAO-A and MAO-B) are important FAD-dependent enzymes (flavoenzymes) responsible for the metabolism of neurotransmitters, such as dopamine, serotonin, adrenaline, and noradrenaline and for the inactivation of exogenous arylalkylamines. Increasing evidence suggests that levels of monoamine oxidase-B (MAO-B) activity could increase up to 3-fold in the temporal, parietal, and frontal cortex of AD patients. The excess MAO-B produces hydroxyl radicals, which could increase the former of Aβ plaques[5]. Thus, a selective MAO-B inhibitor would be a potential strategy for treating AD. Fortunately, selective MAO-B inhibitor rasagiline has been performed in a clinical trial in people with mild-to-moderate AD[6].

The inflammatory hypothesis states that inflammation is considered to be a major factor in AD whereby the beta-amyloid plaques and neurofibrillary tangles co-localize with astrocytes and microglia as well as local immune cells in the brain. In AD, the primary driver of activation of microglia is the accumulation of Aβ. Activated microglia respond to Aβ resulting in migration to the plaques and phagocytosis of Aβ. This results in an accumulation of Aβ and sustained pro-inflammatory cytokine singling beginning to damage neurons[7]. In addition, the excessive accumulation of reactive oxygen species (ROS) in patients with AD induces oxidative stress and further aggravates the production and aggregation of Aβ oligomer[8]. Thus, modulation of inflammation or preventing the formation of the free radicals has been one of the most dynamic areas in the search for new therapeutic targets for AD.

Given the multifactorial aetiology of AD, the development of multi-target-directed ligands (MTDLs) has been considered the best pharmacological option for addressing the progression of AD[9–11]. These MTDLs possess two or more complementary biological activities, and several candidates with disease-modifying potential are now in the pipeline and have completed clinical trials, such as masitinib mesylate (Angiogenesis inhibitors/Lyn kinase inhibitors/Fibroblast growth factor receptor 3 inhibitors/Signal transduction modulators/KIT inhibitors/Tyrosine kinase inhibitors), leuco methylthioninium (microtubule-associated protein tau aggregation inhibitors/MAO inhibitors/Nitric oxide (NO) production inhibitors), blarcamesine hydrochloride (Signal transduction modulators/Muscarinic M1 receptor agonists/sigma non-opioid intracellular receptor 1 agonists/Drugs acting on NMDA receptors/Drugs acting on sodium channels/Lipid peroxidation inhibitors) and troriluzole hydrochloride (Glutamate release inhibitors/Voltage-gated sodium channel blockers/signal transduction modulators/K(V) 4.3 channel blockers) have reached a testing stage in clinical phase II/III trials (Figure 1)[12].

Ferulic acid (FA) is a polyphenol that is abundant in vegetables and maize bran. Several lines of evidence have displayed that FA would be hopeful for treating AD because of its scavenging free radicals, Aβ aggregation inhibition properties, anti-inflammatory properties, and neuroprotective effects[13,14]. However, the low bioavailability of FA limits its clinical uses in AD. Based on this, many groups have developed the FA derivative to treat AD[14]. Rasagiline, a selective MAO-B inhibitor, which has been approved for treating symptoms of Parkinson's disease, is in Phase II clinical trial with mild to moderate AD, the data showed that Rasagiline improved blood flow in a separate small study of 11 people with AD treated for a median of 1.7 years with 1 mg per day, along with donepezil[6]. The propargyl group has been confirmed as the pharmacophore of rasagiline. In addition, evidences show that introducing benzyl derivatives and alkyl fragment into the skeleton could increase MAO-B inhibitory potency[15]. Thus, we plan to introduce the propargyl, benzyl, and alkyl fragment into the FA skeleton based on the MTDLs strategy and create novel *O*-alkyl ferulamide derivatives as multifunctional agents (Figure 2).

Herein, a series of novel *O*-alkyl ferulamide derivatives are designed and synthesised. The *in vitro* biological activities of target compounds are evaluated through MAO-A/MAO-B inhibition, anti-inflammatory property, anti-Aβ aggregation, and neuroprotective effects. Further, the optimised compound is studied in depth by PET-CT imaging.

2. Results and discussion

2.1. Chemistry

The synthetic of novel *O*-alkyl ferulamide derivatives **5a–5i** was described in Scheme 1, the starting material FA (**1**) was with secondary amine NR^1R^2 (**2a–2c**) in the presence of EDCI and HOBt to get key intermediate **3a–3c**[16], yield from 40–56%. Finally, compounds **3a–3c** were treated with halogenated hydrocarbons (R-X) including propargyl bromide (**4a**), CH_3I (**4b**), benzyl bromide (**4c**), cyclohexyl bromide (**4d**), respectively, to obtain the target compounds **5a–5i**, yield from 39–76%. All the target compounds were confirmed by ^{1}H NMR and HR-ESI-MS, and most of them were characterised by ^{13}C NMR.

2.2. huMAO-A and huMAO-B inhibitory activities

The inhibition potency of compounds **5a–5j** towards *hu*MAO-A and *hu*MAO-B were evaluated through fluorescence assay[17,18]. Rasagiline mesylate was also assessed as a positive compound. As

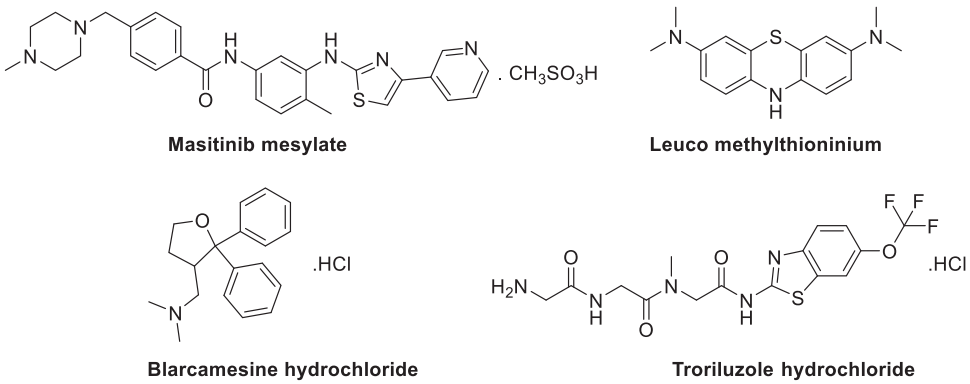

Figure 1. Candidates have reached testing stage in clinical phase II/III trials.

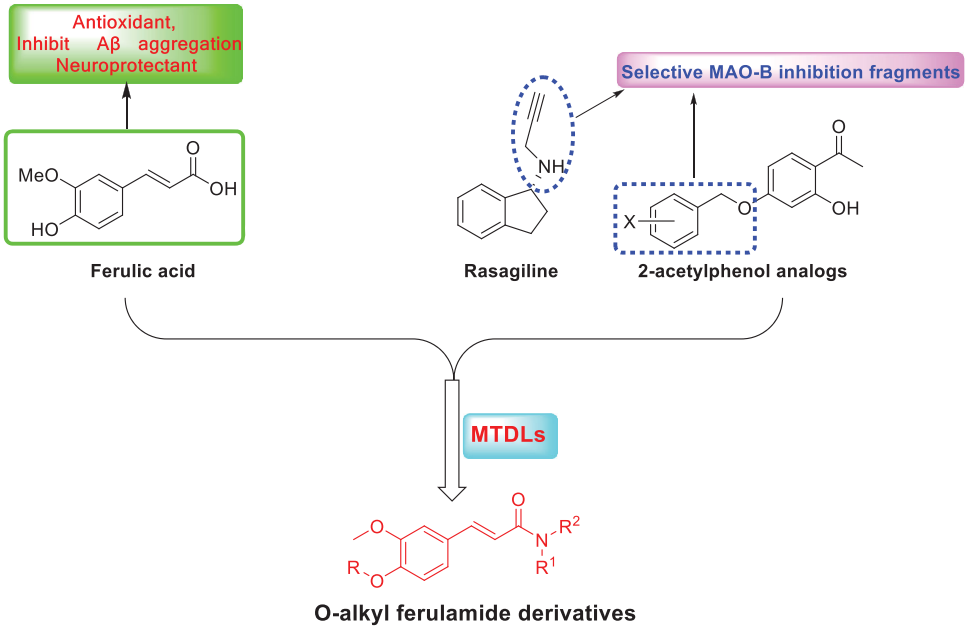

Figure 2. Design strategy of 2-acetylphenol-*O*-alkylhydroxyethylamine derivatives.

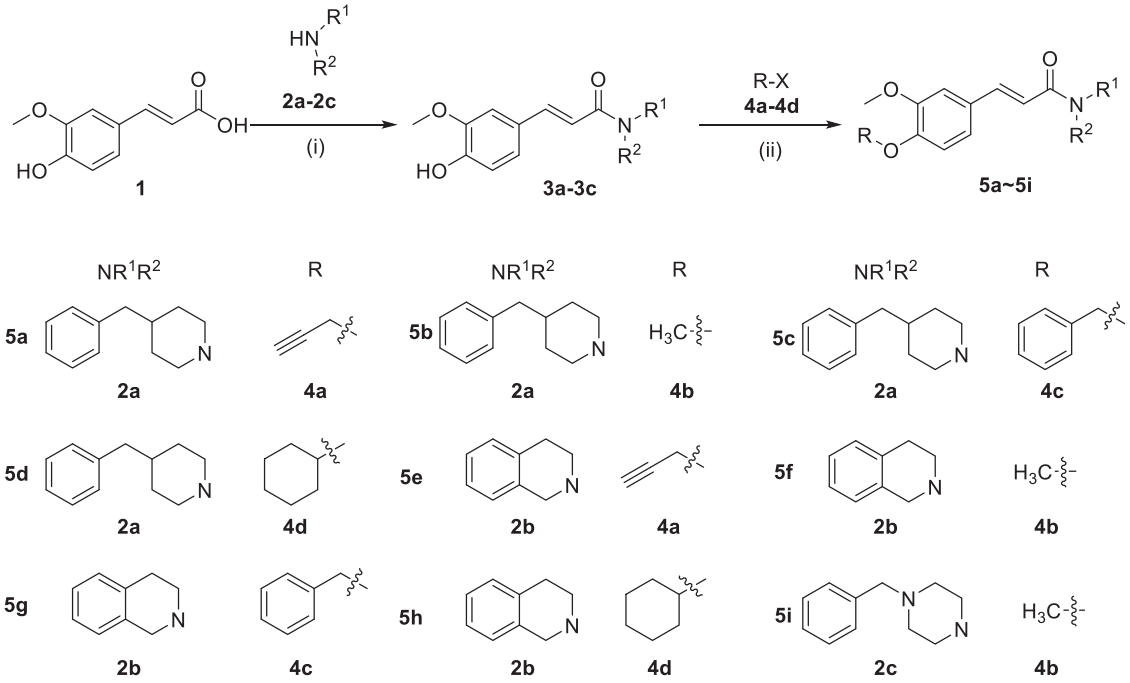

Scheme 1. Synthesis of **5a–5i**. Reagents and conditions: (i) CH_2Cl_2, EDCI, HOBT, room temperature, overnight, yield 40–56%. (ii) RX (**4a–4d**), K_2CO_3, CH_3CN, 65 °C, 6–10 h, yield 39–76%.

listed in Table 1, the positive drug rasagiline mesylate showed excellent *hu*MAO-B inhibitory activity (IC_{50} = 0.03 μM) and good *hu*MAO-A inhibitory activity (IC_{50} = 0.63 μM), which were consistent with the references. All the target compounds showed good *hu*MAO-B inhibitory potency with IC_{50} values ranging from 3.8 μM to 0.32 μM, while displayed weak *hu*MAO-A inhibitory activity. Among them, compound **5a** presented the best selective MAO-B inhibitory activity (IC_{50} = 0.32 μM). The results showed that both the secondary amine NR_1R_2 and alkyl fragment significantly influenced MAO-B inhibitory activity. To explore the inhibition potency of alkyl fragment, firstly NR_1R_2 was fixed with benzylpiperidine (**2a**), compound **5a** with propargyl fragment showed good MAO-B inhibitory potency with an IC_{50} value of 0.32 μM. When changing propargyl fragment of **5a** with a methyl group or benzyl fragment to get compounds **5b** and **5c**, respectively, the MAO-B inhibitory activity decreased to 1.1 and 3.8 μM, respectively, suggesting that the propargyl fragment contributed to the MAO-B inhibitory activity, which was consistent with the previous work[19]. Then, when changing propargyl fragment of **5a** with cyclohexyl group to get compound **5d**, the MAO-B inhibitory activity slightly decreased to 0.56 μM. Further, when NR_1R_2 was fixed with 1,2,3,4-tetrahydroisoquinoline fragment, the similar inhibition tendency of alkyl fragment was also observed, such as compound **5e** with propargyl (IC_{50} = 0.54 μM) > compound **5f** with methyl (IC_{50} = 0.73 μM) > compound **5h** with cyclohexyl (IC_{50} = 0.73 μM) > compound **5g** with benzyl (IC_{50} = 3.1 μM). On the other side, the NR_1R_2 fragment

Table 1. Inhibitory activity of MAO-A/MAO-B, antioxidant activity and effects on self-induced A$\beta_{1\text{-}42}$ aggregation by target compounds and positive compounds.

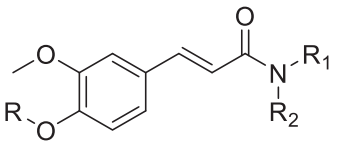

			IC50 ± *SD* (μM)[a]				Self-induced Aβ1-42 aggregation (%)	
Compd	NR1R2	*R*	hMAO-A	hMAO-B	SI[c]	ORAC[d]	Inhibition[e]	Disaggregation[f]
5a	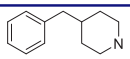 **2a**	 **4a**	45.2 ± 1.3	0.32 ± 0.02	141	0.4 ± 0.01	52.3 ± 1.3	40.1 ± 1.5
5b	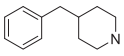 **2a**	H_3C- **4b**	66.1 ± 2.7	1.1 ± 0.07	60	0.3 ± 0.05	n.t.[g]	n.t.[g]
5c	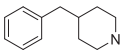 **2a**	 **4c**	80.7 ± 3.9	3.8 ± 0.09	21	0.2 ± 0.03	n.t.[g]	n.t.[g]
5d	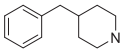 **2a**	 **4d**	63.9 ± 5.1	0.56 ± 0.01	114	0.3 ± 0.03	59.6 ± 2.7	47.2 ± 2.3
5e	 **2b**	 **4a**	64.0 ± 2.9	0.54 ± 0.05	118	0.2 ± 0.03	63.5 ± 3.4	43.8 ± 1.9
5f	 **2b**	H_3C- **4b**	11.3 ± 0.08%[b]	0.73 ± 0.06	—	0.3 ± 0.02	61.7 ± 2.1	45.9 ± 3.6
5g	 **2b**	 **4c**	20.6 ± 0.15%[b]	3.1 ± 0.23	—	0.4 ± 0.02	n.t.[g]	n.t.[g]
5h	 **2b**	 **4d**	65.3 ± 3.4	0.86 ± 0.09	76	0.2 ± 0.03	n.t.[g]	n.t.[g]
5i	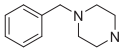 **2d**	H_3C- **4b**	63.2 ± 4.5	1.9 ± 0.18	33	0.7 ± 0.02	n.t.[g]	n.t.[g]
FA			n.t.[g]	n.t.[g]		1.5 ± 0.08	30.6 ± 1.2	48.3 ± 2.6
rasa.[h]			0.63 ± 0.05	0.03 ± 0.004		n.t.[g]	n.t.[g]	n.t.[g]
Curc.[i]			n.t.[g]	n.t.[g]		n.t.[g]	46.1 ± 1.3	56.7 ± 1.8

[a]IC_{50}: 50% inhibitory concentration. The experiment was performed through three independent experiments, and result were presented as the mean ± SEM.
[b]MAO-A inhibition rate was tested at 62.5 μM.
[c]SI = selectivity index = IC_{50} (hMAO-A)/IC_{50} (hMAO-B).
[d]The experiment was performed using ORAC assay, results are expressed as μM of Trolox equivalent/μM of tested compound.
[e]Inhibition of self-induced A$\beta_{1\text{-}42}$ aggregation using ThT assay, the inhibition rate was obtained at 25 μM for both tested compounds and A$\beta_{1\text{-}42}$, data are presented as the mean ± SEM.
[f]Disaggregation of A$\beta_{1\text{-}42}$ aggregates, the concentration of tested compounds and A$\beta_{1\text{-}42}$ were 25 μM.
[g]n.t.: not tested.
[h]rasa.: rasagiline mesylate.
[i]Curc.: Curcumin.

also affected MAO-B inhibitory activity. When the alkyl fragment was propargyl (**4a**), compound **5a** with benzylpiperidine (**2a**) fragment showed good MAO-B inhibitory activity with an IC_{50} value was 0.32 μM. When changing benzylpiperidine (**2a**) fragment with 1,2,3,4-tetrahydroisoquinoline (**2b**) to get compound **5e**, the MAO-B inhibitory activity decreased to 0.54 μM. Subsequently, when the alkyl fragment was methyl, compound **5b** with benzylpiperidine showed good MAO-B inhibitory potency (IC_{50} = 1.1 μM). When changing benzylpiperidine of **5b** with 1,2,3,4-tetrahydroisoquinoline to get compound **5f**, the MAO-B inhibitory activity slightly increased to 0.73 μM. When changing benzylpiperidine of **5b** with benzylpiperazine to get compound **5i**, the MAO-B inhibitory activity decreased to 1.9 μM. Overall speaking, compounds **5a**, **5d**, **5e**, **5f**, and **5h** presented good selective MAO-B inhibitory potency, deserving further study.

2.3. Kinetic studies for huMAO-B

Compound **5a** was selected to perform the kinetic study against *hu*MAO-B using Lineweaver-Burk plots assay[20]. As displayed in Figure 3, the Lineweaver-Burk plots for three concentrations of **5a** were linear and intersected at *y*-axis. These results indicated that **5a** was a competitive MAO-B inhibitor.

2.4. Molecular modelling study of MAO-B

From the above data, compound **5a**, a good selective MAO-B inhibitor, was selected to further explore the binding mode with MAO-B (PDB code: 2V60) through a molecular docking[21]. In **5a**-MAO-B complex (Figure 4(A)), the benzene ring of benzylpiperidine interacted with key residue Tyr435 via Pi-Pi interaction. The Tyr435 residue was a key amino acid in the active site of MAO-B (PDB ID: 2v60), in the structure of human MAO-B in complex with the selective inhibitor 7–(3-chlorobenzyloxy)-4-carboxaldehyde-coumarin from PBD database (Figure 4(B)), the aldehyde group interacted with residue Tyr435 via one intermolecular hydrogen bonding. In addition, Figure 4(A) showed that the O atom of the carbonyl group interacted with key residue Tyr326 and Gln206 via one intermolecular hydrogen bonding, respectively. Moreover, the CH = CH fragment interacted with key amino acid Tyr326 via one Sigma-Pi interaction. Besides, there were some hydrophobic interactions that could be observed between the ligand **5a** and amino acids Leu164, Pro104, Phe103, Ile199, Gln206, Leu171, Phe 343, and Tyr326. Similarly, the hydrophobic interactions were also observed between the ligand and residues Leu164, Pro104, Ile199, Gln206, Leu171, Phe 343, and Tyr326 in Figure 4(B). Thus, the observed interactions offered a rational explanation for the high MAO-B inhibitory activity towards **5a**.

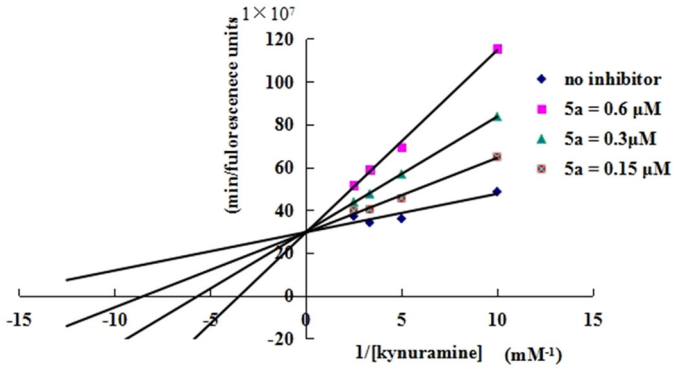

Figure 3. Linewear-Burk plots resulting from the subvelocity curve of the MAO-B activity different substrate concentration in the absence and presence of **5a** (0.15, 0.3, and 0.6 μM).

2.5. Antioxidant activity assay

The antioxidant activity of synthesised compounds **5a–5i** was tested by oxygen radical absorbance capacity fluorescein (ORAC-FL) assay, FA was also tested as a referenced compound[22,23]. As presented in Table 1, FA showed good antioxidant activity with an ORAC value of 1.5 *eq*. Correspondingly, compounds **5a–5i** displayed moderate to good antioxidant potency with ORAC value of 0.2–0.7 *eq*. Generally speaking, compound **5i** (ORAC = 0.7 *eq*) with benzylpiperazine fragment showed better antioxidant activity than other derivatives. The benzylpiperidine, 1,2,3,4-tetrahydroisoquinoline, and alkyl fragments did not produce a significant influence on the antioxidant activity of the target compounds.

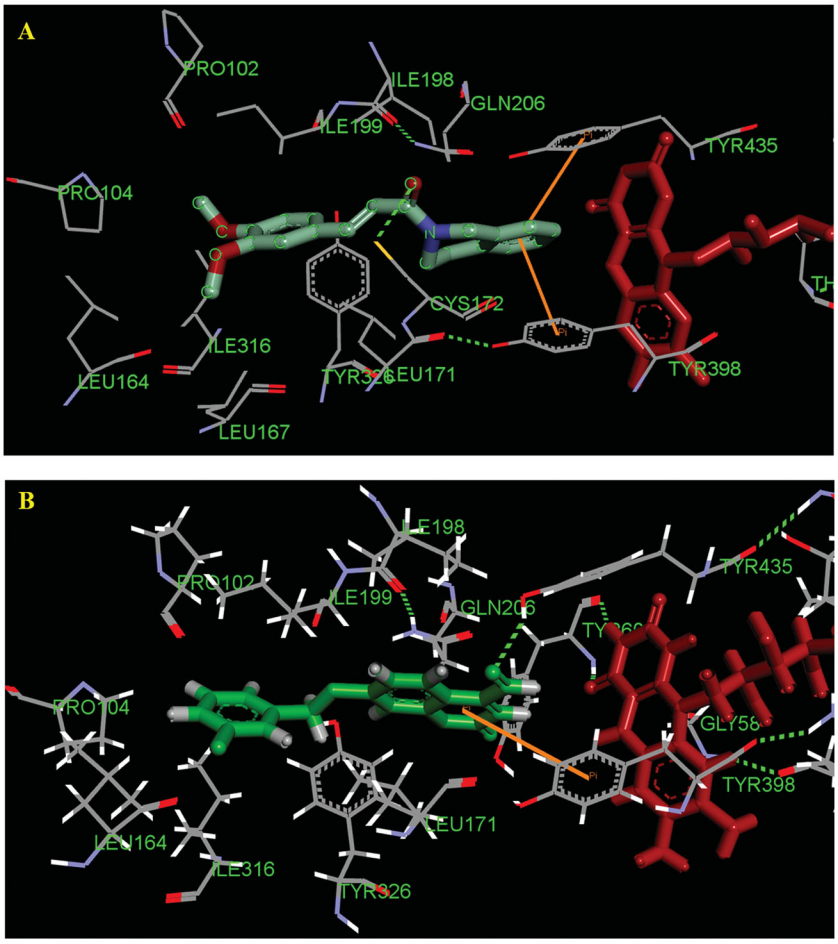

Figure 4. (A) Compound **5a** (green stick) interacted with residues in the binding site of *h*MAO-B (PDB code: 2V60). (B) The selective inhibitor 7-(3-chlorobenzyloxy)-4-carboxaldehyde-coumarin interacted with residues in the binding site of *h*MAO-B (PDB code: 2V60).

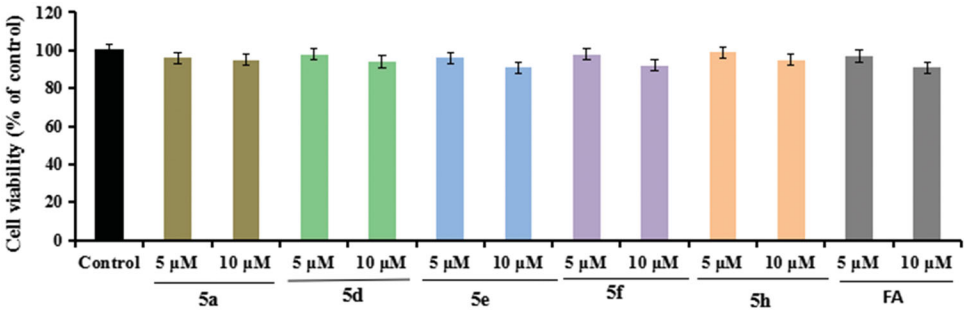

Figure 5. The cell viability of compounds **5a**, **5d**, **5e**, **5f**, **5h**, and FA on the BV-2 cells were testing using MTT assay. The data were expressed as the mean ± *SD* through three independent experiments.

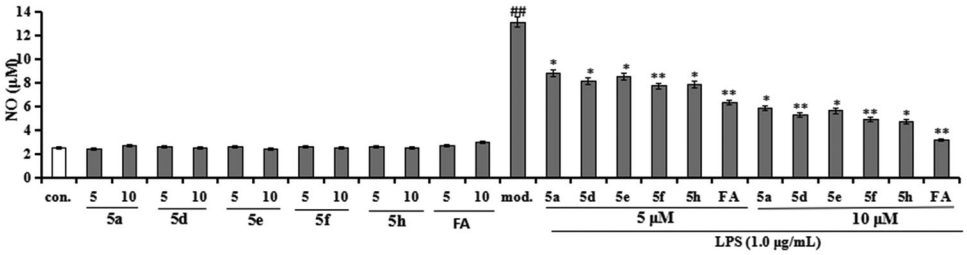

Figure 6. Effects of compounds **5a**, **5d**, **5e**, **5f**, **5h**, and FA on NO release in BV-2 cells and LPS-stimulated BV-2 cells. Data were expressed as mean ± *SD* through three independent experiments. con. = control; mod. = model. $^{\#\#}p < 0.01$ *vs.* control; $^{**}p < 0.01$, $^{*}p < 0.05$ *vs.* LPS-induced group.

2.6. Anti-inflammatory property

Based on the results of MAO-B inhibitory activity, compounds **5a**, **5d**, **5e**, **5f**, and **5h** showed good MAO-B inhibitory potency, which was selected to test the anti-inflammatory potency by measuring the production of inflammatory mediators TNF-α and NO in LPS-induced BV-2 cells[21,24].

2.6.1. Cytotoxicity of compounds 5a, 5d, 5e, 5f, and 5h on BV-2 cells

The cytotoxicity of compounds **5a**, **5d**, **5e**, **5f**, and **5h** were tested using MTT assay, and FA was also tested for comparison. As shown in Figure 5, the cell viability did not show obvious change after adding compounds **5a**, **5d**, **5e**, **5f**, **5h**, and FA (5 μM and 10 μM), showing that compounds **5a**, **5d**, **5e**, **5f**, **5h**, and FA were non-toxic on BV-2 cells at 5 and 10 μM, respectively.

2.6.2. Evaluation of NO and TNF-α in LPS-stimulated BV-2 cells

The inhibition of NO production was tested on LPS-induced BV-2 cells through the Griess reaction method[24]. As displayed in Figure 6, the release volume of NO did not produce obvious change after adding tested compounds (**5a**, **5d**, **5e**, **5f**, **5h**, and FA) at the concentration of 5 and 10 μM, respectively, exhibiting that the tested compounds did not produce an effect on the release of NO in BV-2 cells. When BV-2 cells were treated with LPS (1 μg/mL), the release volume of NO remarkably increased. Moreover, when the BV-2 cells were pre-treated with compounds **5a**, **5d**, **5e**, **5f, 5h**, and FA at 5 μM, leading to a remarkable reduction of LPS-induced NO production with 32.8, 38.1, 35.1, 41.2, 40.4, and 51.9% inhibition rate, respectively. And when pre-treatment with compounds **5a**, **5d**, **5e**, **5f**, **5h**, and FA at 10 μM, the inhibition rate significantly improved to 55.7, 59.5, 57.3, 62.5, 64.1, and 75.6%, respectively. In addition, the effects of compounds **5a**, **5d**, **5e**, **5f**, and **5h** on LPS-induced TNF-α production in BV-2 cells were determined using the enzyme-linked immunosorbent assay (ELISA). As displayed in Figure 7, when BV-2 cells were exposed to 1.0 μg/mL LPS, the levels of TNF-α significantly increased to 1880 pg/mL ($p < 0.01$) compared with the untreated group (140 pg/mL). When treatment with tested compounds (**5a**, **5d**, **5e**, **5f**, **5h**, and FA) at 5 μM, respectively, the levels of TNF-α production decreased to 820 pg/mL ($p < 0.05$), 780 pg/mL ($p < 0.01$), 805 pg/mL ($p < 0.05$), 750 pg/mL ($p < 0.01$), 740 pg/mL ($p < 0.01$), and 539 pg/mL ($p < 0.01$), respectively, and the inhibitory rate were 51.7, 54.1, 52.6, 55.9, 56.5, and 68.3%, respectively. When treatment with tested compounds (**5a**, **5d**, **5e**, **5f**, **5h**, and FA) at 10 μM, respectively, the levels of TNF-α production decreased to 520 pg/mL ($p < 0.05$), 460 pg/mL ($p < 0.01$), 550 pg/mL ($p < 0.05$), 455 pg/mL ($p < 0.01$), 435 pg/mL ($p < 0.01$) and 234 pg/mL ($p < 0.01$), respectively. The above results showed that compounds **5a**, **5d**, **5e**, **5f**, and **5h** could reduce the release of NO and suppress TNF-α production in LPS-induced BV-2 cells, and presented lower anti-neuroinflammatory potency *in vitro* than the skeleton FA.

2.7. Effects on self-induced $A\beta_{1-42}$ aggregation

There were two experiments were performed: inhibition experiments and disaggregation experiments[22,25]. Based on the above results, the potent compounds **5a**, **5d**, **5e**, **5f**, and **5h** were selected to test the inhibition effects against self-induced $A\beta_{1-42}$ aggregation by thioflavin T (ThT) fluorescence assay, as well as FA and curcumin acted as positive compounds. As listed in Table 1, compounds **5a**, **5d**, **5e**, **5f**, and **5h** showed significant inhibitory potency against self-induced $A\beta_{1-42}$ aggregation with 52.3, 59.6, 63.5, and 61.7% inhibition rates at 25 μM, respectively, which were better than FA (30.6%) and curcumin (46.1%). Further, the transmission electron microscopy (TEM) images in Figure 8(A) also supported the results from the ThT assay.

For the disaggregation experiment, the obtained data in Table 1 displayed that compounds **5a**, **5d**, **5e**, **5f**, and **5h** presented potent disaggregation potency with 40.1, 47.2, 43.8, 45.9% disaggregation rates, respectively, which were also supported by TEM images in Figure 8(B).

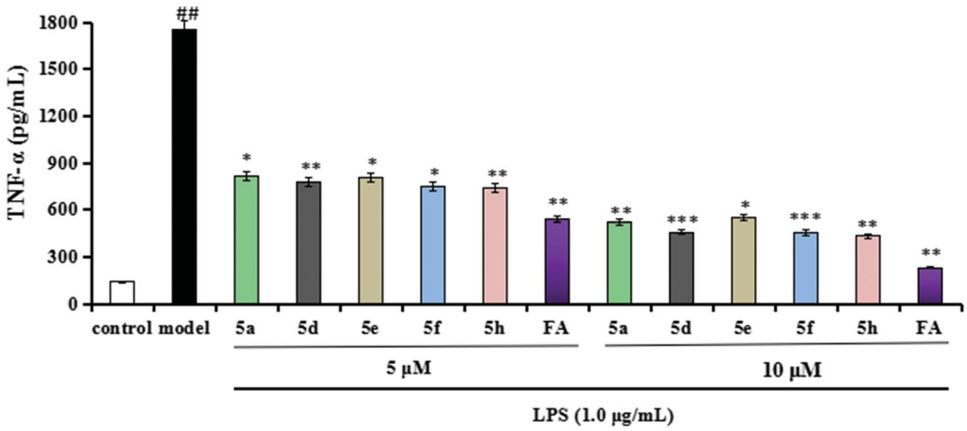

Figure 7. Effects of compounds **5a**, **5d**, **5e**, **5f**, **5h**, and FA on TNF-α release in LPS-stimulated BV-2 cells. Data were expressed as mean ± *SD* through three independent experiments. $^{\#\#}p < 0.01$ *vs.* control; $^{***}p < 0.01$, $^{**}p < 0.01$, $^{*}p < 0.05$ *vs.* LPS-induced group.

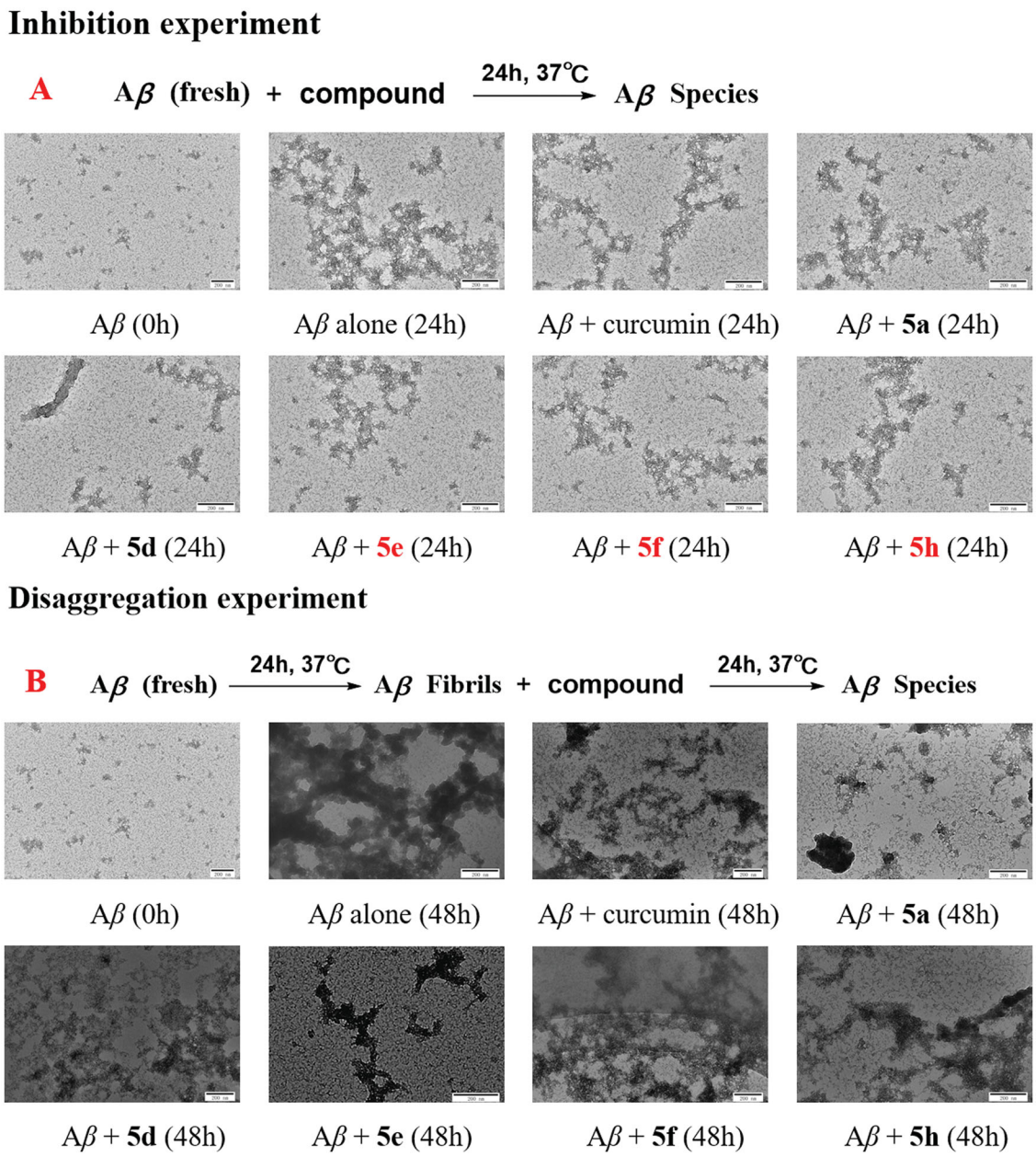

Figure 8. TEM images of Aβ species. (A) inhibition experiments of self-induced $A\beta_{1-42}$ aggregation. (B) disaggregation experiments of self-induced $A\beta_{1-42}$ aggregation.

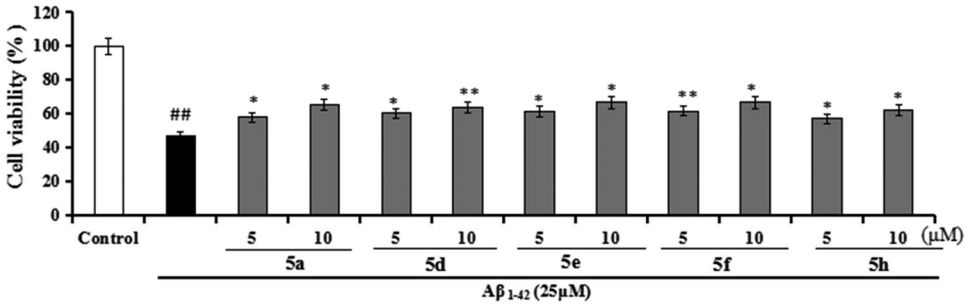

Figure 9. The cell viability (%) of compounds **5a**, **5d**, **5e**, **5f**, and **5h** on A$\beta_{1\text{-}42}$-induced PC12 cell injury by MTT assay. Percentages of the cell viability were presented as mean ± *SD* from three independent experiments. $^{\#\#}p < 0.01$ *vs.* untreated group; $^{**}p < 0.01$, $^{*}p < 0.05$ *vs.* A$\beta_{1\text{-}42}$-induced group.

Table 2. Permeability ($P_e \times 10^{-6}$ cm/s) in the PAMPA-BBB assay for 11 commercial drugs used in the experiment validation.

Commercial drugs	Bibl[a]	PBS:EtOH (70:30)[b]
Verapamil	16	16.90
Oxazepam	10	9.60
Diazepam	16	11.86
Clonidine	5.3	5.10
Imipramine	13	10.10
Testosterone	17	16.30
Caffeine	1.3	1.28
Enoxacine	0.9	0.47
Piroxicam	2.5	0.72
Norfloxacin	0.1	0.42
Theophylline	0.12	0.10

[a]Taken from Ref[28].
[b]Data are the mean ± *SD* of three independent experiments.

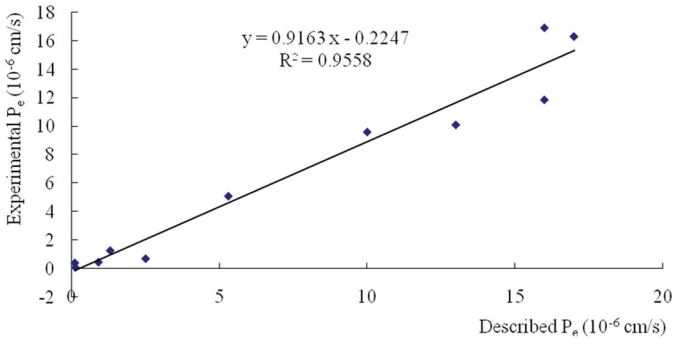

Figure 10. Linear correlation between experimental and reported permeability of commercial drugs using the PAMPA-BBB assay. P_e(exp) = 0.9163, P_e(bibl.) −0.2247 (r^2 = 0.9558).

2.8. Neuroprotective effects against Aβ-induced PC12 cell injury

To consolidate the results obtained from the inhibition studies of self-induced A$\beta_{1\text{-}42}$ aggregation, further study was performed to evaluate the neuroprotective effect of compounds **5a**, **5d**, **5e**, **5f**, and **5h** against PC12 cell injury induced by A$\beta_{1\text{-}42}$ using MTT assay[26]. Two different concentrations (5 and 10 μM) of each compound were employed in this experiment. As displayed in Figure 9, when the PC12 cells were treated with 25 μM A$\beta_{1\text{-}42}$ for 48 h, the cell viability decreased to 47.5% ($p < 0.01$) compared with the control group. When treated with compound **5a**, the cell viability was 58.2 and 63.7%, respectively. Similarly, when treating with compounds **5d**, **5e**, **5f**, and **5h**, respectively, the cell viability gradually increased in a dose-dependent manner, showing compounds **5a**, **5d**, **5e**, **5f**, and **5h** presented a potent neuroprotective effect against A$\beta_{1\text{-}42}$-induced PC12 cell injury.

2.9. In vitro *blood – brain barrier permeability*

The blood-brain barrier (BBB) permeability is an important factor for the development of anti-CNS drugs, herein the ability of compounds **5a**, **5d**, **5e**, **5f**, and **5h** to access BBB was evaluated by the parallel artificial membrane permeation assay of the blood – brain barrier (PAMPA-BBB)[25,27]. 11 commercial drugs were employed to verify this assay (Table 2). A plot of the experimental data versus the reported values produced a good linear correlation, P_e (exp) = 0.9163P_e (bibl.) − 0.2247 (r^2 = 0.9558) (Figure 10). From this equation, and considering the limit established by Di et al. for blood – brain barrier permeation, the following ranges of permeability P_e ($\times 10^{-6}$ cm/s) were established: $P_e > 3.44$ for compounds with high BBB permeation; $3.44 > P_e > 1.61$ showed uncertain BBB permeation; $P_e < 1.61$ showed weak BBB permeation. As displayed in Table 3, compounds **5a**, **5d**, **5e**, **5f**, and **5h** presented good BBB permeation with 14.7×10^{-6}, 18.2×10^{-6}, 12.5×10^{-6}, 20.4×10^{-6}, and 16.7×10^{-6} cm/s permeability, respectively, as similar with testosterone and diazepam, displaying that compounds **5a**, **5d**, **5e**, **5f**, and **5h** could cross BBB through passive diffusion and deserving further investigation.

Table 3. The predictive permeation of compounds **5a**, **5d**, **5e**, **5f**, and **5h** by PAMPA-BBB assay.

Compound	P_e ($\times 10^{-6}$ cm/s)	Prediction
Testosterone	17.3 ± 0.3	CNS+
Diazepam	15.2 ± 0.5	CNS+
Norfloxacin	0.13 ± 0.01	CNS-
5a	14.7 ± 0.76	CNS+
5d	18.2 ± 0.79	CNS+
5e	12.5 ± 0.66	CNS+
5f	20.4 ± 0.81	CNS+
5h	16.7 ± 0.59	CNS+

2.10. Theoretical prediction of the ADME properties

The drug-like properties of compounds **5a**, **5d**, **5e**, **5f**, and **5h** were evaluated using the Molinspiration property program[28]. A widely accepted method to predict ADME properties is the Rule of Five proposed by Lipinski in 1997. The items of Rule of Five were that octanol-water partition coefficient (log *P*) <5, molecular weight (MW) <500, number of hydrogen-bond donors (n-OHNH) <5, number of hydrogen-bond acceptors (n-ON) <10, number of rotatable bonds ≤10, and the rotatable bonds were single bonds that are not adjacent to triple bonds, do not connect hydrogen or halogen atoms and are not included in rings containing <5 single bonds. Topological Polar Surface Area (TPSA), for the CNS drugs, TPSA ≤90 Å^2. As demonstrated in Table 4, compounds **5a**, **5d**, **5e**, **5f**, and **5h** complied with the Rule of Five, deserving further investigations.

Table 4. Theoretical prediction of the druglike properties of compounds **5a**, **5d**, **5e**, **5f**, and **5h**.

Compound	Log *P*	MW	TPSA (Å^2)	n-ON	n-OHNH	nviolations	nrotb	volume (Å^3)
5a	4.4	389.50	38.78	4	0	0	7	378.22
5d	6.14	433.59	38.78	4	0	1	7	429.16
5e	3.21	347.41	38.78	4	0	0	5	327.79
5f	3.05	323.39	38.78	4	0	0	4	305.29
5h	4.96	391.51	38.78	4	0	0	5	378.73

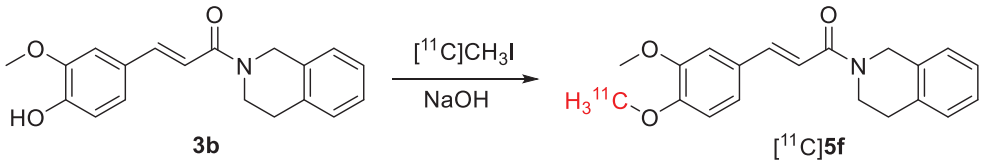

Scheme 2. Radiosynthesis of [^{11}C]**5f**. Reagents and conditions: NaOH, DMF, 100 °C, 3 min.

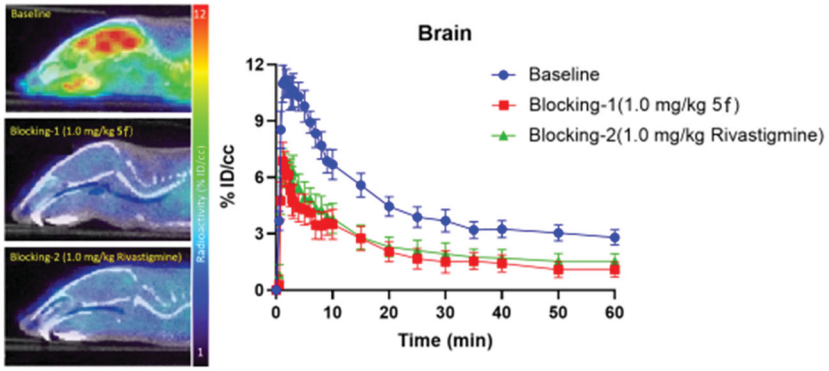

Figure 11. PET/CT (baseline and blocking) images in mice brain (20–60 min) with [^{11}C]**5f** after intravenous administration (i.v.) and time-activity curve of the whole brain ($n = 4$).

2.11. In vivo *PET-CT imaging with [^{11}C]5f in mice*

To further explore the BBB permeation of the *O*-alkyl ferulamide derivatives, compound **5f** was selected to evaluate using PET-CT imaging in mice.

2.11.1. *Preparation of the precursor and radiosynthesis of [^{11}C]5f*[29,30]

Precursor **3b** was used as the [^{11}C]**5f** preparation (Scheme 2). [^{11}C]**5f** was obtained from the methylation of **3b** by reacting with [^{11}C]CH_3I in the presence of sodium hydroxide. The radio-desired product was collected by injecting it into the semi-preparative reversed-phase HPLC and was reformulated by loading it onto solid-phase exchange (SPE) C-18 cartridges. The preparation process of [^{11}C]**5f** was accomplished in 30–40 min after the end of bombardment (EOB), with an overall non-decay corrected radiochemical yields (12–15%) at the end of synthesis (EOS) and high specific activity of 83.2 GBq/μmol (EOB).

2.11.2. In vivo *PET-CT imaging with [^{11}C]5f in mice*

Preliminary rodent PET/CT imaging studies were performed to investigate the *in vivo* bio-distribution of [^{11}C]**5f**. 60-min dynamic PET scans were conducted after the tail vein injection of [^{11}C]**5f** in mice. The radioactivity was presented as the percentage of injected dose per unit volume (% ID/cc). Representative mice brain PET/CT images with [^{11}C]**5f** are shown in Figure 11. Encouragingly, the results demonstrated that [^{11}C]**5f** could penetrate the BBB with a high brain uptake. From the time-activity curve (TAC) analysis in the whole brain, [^{11}C]**5f** reached a maximum uptake of 11.2%ID/cc in the first few minutes after injection and exhibited good brain clearance kinetic properties during the 60-min scanning time.

Further blocking studies were performed to verify the specific binding of [^{11}C]**5f** (Figure 11). The anti-AD drug Rivastigmine approved by FDA was performed. Unlabelled [^{11}C]**5f** (1.0 mg/kg, self-blocking) and Rivastigmine (1.0 mg/kg) were pre-treated 5 min before the radiotracer administration. Compared with the bassline, a significant radio-uptake decrease (~35%) in the brain was observed in both **5f** and Rivastigmine pre-treated mice, indicating specific binding of [^{11}C]**5f**.

The *in vivo* whole-body distribution of [^{11}C]**5f** was analysed at several scan time points (5, 15, 30, and 60 min). The mean radioactivity uptake in the organs of interest at each time point is presented in the histogram (Figure 12). The uptake of [^{11}C]**5f** reached the highest concentration after injection at 5 min in the heart (14.20 ± 0.18%ID/cc), lung (9.5 ± 0.15%ID/cc), and spleen (11.4 ± 0.11%ID/cc) and gradually washed out from these organs. A high accumulation of radioligand was found in the liver and kidney, where the radioactivity steadily increased over time and achieved a maximum of 24.3 ± 0.16%ID/cc and 18.7 ± 0.13%ID/cc, respectively. The relatively high uptake in the liver and kidney indicated that [^{11}C]**5f** is primarily excreted through the hepatobiliary and urinary pathways.

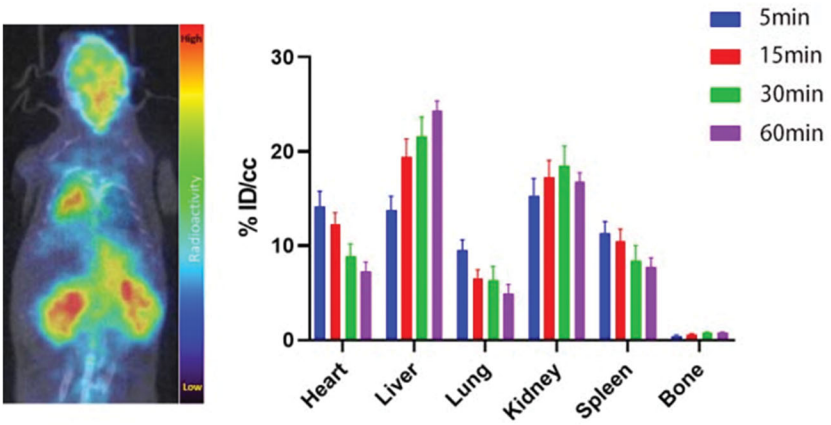

Figure 12. Left: the PET/CT imaging of the mice with [^{11}C]**5f** (whole body, 0–60 min); right: biodistribution of [^{11}C]**5f** in organs of interest at 5, 15, 30, and 60 min after injection of radioligand ($n = 4$ for each time point). Error bars represent SEM.

3. Conclusion

AD, accounting for about 70% of all dementia cases, is a chronic, progressive neurodegenerative brain disease in elderly people. There are more than 50 million people living with dementia worldwide and the figure of AD patients will triple by 2050. Accordingly, AD poses a great problem for global health. The current therapeutic agents approved by FDA, including AChE inhibitors (rivastigmine, donepezil, and galantamine) and the NMDA receptor antagonist (menantine), only present modest symptomatic effects and cannot stop, prevent, or reverse the progression of AD. Thus, the development of disease-modifying drugs is a great unmet medical need for AD patients.

Given the complexity of AD, the MTDLs strategy was considered the most promising strategy for the treatment of AD. In this work, based on the MTDLs strategy, a series of novel *O*-alkyl ferulamide derivatives were designed by introducing propargyl fragments into ferulic acid skeleton. The target compounds were synthesised and evaluated by MAO-A/MAO-B inhibition, antioxidant activity, anti-inflammatory property, anti-Aβ aggregation, and neuroprotective effects. The results *in vitro* displayed that all the target compounds were highly selective MAO-B inhibitors, and both the secondary amine NR_1R_2 and alkyl fragment significantly influenced MAO-B inhibitory activity. Among them, compounds **5a**, **5d**, **5e**, **5f**, and **5h** presented significantly selective MAO-B inhibitory potency with IC_{50} values of 0.32, 0.56, 0.54, 0.73, and 0.86 μM, respectively. Furthermore, compounds **5a**, **5d**, **5e**, **5f**, and **5h** indicated potential anti-inflammatory properties by reducing the release of NO and suppressing TNF-α production in LPS-induced BV-2 cells. Compounds **5a**, **5d**, **5e**, **5f**, and **5h** also showed moderate antioxidants. Moreover, compounds **5a**, **5d**, **5e**, **5f**, and **5h** remarkably inhibited and disaggregated self-induced A$\beta_{1\text{-}42}$ aggregation, which were supported by TEM images, and displayed a potent neuroprotective effect on A$\beta_{1\text{-}42}$-mediated PC12 cell injury. More importantly, compounds **5a**, **5d**, **5e**, **5f**, and **5h** presented good blood–brain barrier permeation *in vitro* and drug-like properties, which was consistent with our design strategy. Further, representative compound **5a** was selected to evaluate the BBB permeability *in vivo*, the PET/CT images analysis with [^{11}C]**5f** displayed that [^{11}C]**5f** could penetrate the BBB with a high brain uptake and exhibited good brain clearance kinetic property, suggesting that compound **5f** presented good BBB permeability and bioavailability compared with ferulic acid. In general, this work provided an effective strategy to improve the BBB permeability and bioavailability of natural products. Moreover, compound **5f** was a potent multi-functional candidate for the treatment of AD and deserved further modification and investigations.

4. Experimental section

4.1. Chemistry

Unless otherwise noted, the reagents required for the chemical synthesis were obtained from Shanghai Titan Scientific Co., Ltd. and were used without purification. All new compounds provided satisfactory ^{1}H NMR and ^{13}C NMR spectra were recorded on a Varian INOVA spectrometer and used $CDCl_3$ as a solvent, referenced to Tetramethylsilane (TMS). Chemical shifts (δ) are reported in ppm. Splitting patterns are designated as s, single; d, doublet; dd, double-doublet; t, triplet; m, multiplet. The purity of the final synthesised products was evaluated by HPLC analyses which were conducted with a Waters X-Bridge C18 column (4.6 mm $\times$ 150 mm, 5 μm) at a flow ratio of 0.8 ml/min. Mobile phase: A: 0.12%TFA in H_2O, B: 0.1% TFA in CH_3CN. The high-resolution mass spectra were obtained by Waters Xevo G2-XS-Qtof mass spectrometer.

4.1.1. General preparation procedures of 3a–3c

The starting material FA **1** (3 mmol) was dissolved in 20 ml of THF. To this solution, EDCI (4.5 mmol), HOBT (4.5 mmol), and secondary amines **2a–2c** (3.5 mmol) were added, respectively, and the reaction mixture was stirred at room temperature overnight. The reaction was monitored through TLC, the solvent was evaporated under reduced pressure after reaction completion. The crude residue was dissolved in 50 ml CH_2Cl_2, washed with water (2 $\times$ 50 ml), saturated NaCl (80 ml), and dried (Na_2SO_4). The resulting crude was purified by silica gel chromatography (CH_2Cl_2/acetone = 50:1) to afford the desired **3a–3c**, which had been reported in our previous work[16].

4.1.1.1. (E)-1-(4-benzylpiperidin-1-yl)-3-(4-hydroxy-3-methoxyphenyl)prop-2-en-1-one (3a). The starting material FA **1** was treated with secondary amine benzylpiperazine **2a** to get intermediate **3a**. White solid, yield 51.5%.

4.1.1.2. (E)-1-(3,4-dihydroisoquinolin-2(1H)-yl)-3-(4-hydroxy-3-methoxyphenyl)prop-2-en-1-one (3b). The starting material FA **1** was treated with secondary amine 1,2,3,4-tetrahydroisoquinoline **2b** to get intermediate **3b**. White solid, yield 53.2%.

4.1.1.3. (E)-1-(4-benzylpiperazin-1-yl)-3-(4-hydroxy-3-methoxyphenyl)prop-2-en-1-one (3c). The starting material FA **1** was treated with secondary amine benzylpiperazine **2d** to get intermediate **3c**. Light yellow oil, yield 55.9%.

4.1.2. General procedures for the synthesis of target compounds 5a–5i

Alkyl halide **4a–4d** (1.3 mmol) was added to a mixture of anhydrous K_2CO_3 (1.2 mmol), and the key intermediate **3a–3c** (1.0 mmol) in 8 ml anhydrous CH_3CN. The reaction mixture was heated to 65 °C and stirred for 6–10 h under an argon atmosphere. The reaction was monitored by TLC. On completion of the reaction, the solvent was evaporated under reduced pressure. The crude residue was treated with 30 ml of water and the mixture was extracted with CH_2Cl_2 (2 × 30 ml). The combined organic phases were washed with saturated NaCl (50 ml), dried over anhydrous Na_2SO_4, and filtered. The solvent was evaporated under reduced pressure and the residue was purified by silica gel chromatography (petroleum ether/acetone = 50:1) to get compounds **5a–5i**.

4.1.2.1. (E)-1-(4-benzylpiperidin-1-yl)-3-(3-methoxy-4-(prop-2-yn-1-yloxy)phenyl)prop-2-en-1-one (5a). Intermediate **3a** was treated with propargyl bromide **4a** to get target compound **5a**. Light yellow oil, 55.2% yield, 97.5% HPLC purity. ^{1}H NMR (400 MHz, $CDCl_3$) δ 7.59 (d, J = 15.3 Hz, 1H, C = CH), 7.29–7.26 (m, 2H, 2 × Ar-H), 7.21 (d, J = 7.2 Hz, 1H, Ar–H), 7.16 − 7.11 (m, 2H, 2 × Ar–H), 7.09 (s, 1H, Ar–H), 7.05 − 6.98 (m, 2H, 2 × Ar–H), 6.77 (d, J = 15.4 Hz, 1H, C = CH), 4.75 (d, J = 1.7 Hz, 2H, OCH_2), 4.70–4.67 (m, 1H, 1/2 $phCH_2$), 4.09–4.06 (m, 1H, 1/2 $phCH_2$), 3.88 (s, 3H, OCH_3), 3.02 (s, 1H, C≡CH), 2.54–2.52 (m, 3H, NCH_2, 1/2NCH_2), 2.31–2.29 (m, 1H, 1/2NCH_2), 1.81–1.76 (m, 1H, CH), 1.72 (d, J = 13.6 Hz, 2H, CH_2), 1.26–1.19 (m, 2H, CH_2). ^{13}C NMR (101 MHz, $CDCl_3$) δ 165.4, 149.7, 148.1, 142.2, 139.9, 129.7, 129.1, 128.3, 126.1, 121.2, 116.0, 115.1, 114.0, 110.6, 78.2, 76.2, 56.7, 56.0, 42.9, 38.3. HR-ESI-MS: Calcd. for $C_{25}H_{27}NO_3$ $[M + H]^+$: 390.2024, found: 390.2066.

4.1.2.2. (E)-1-(4-benzylpiperidin-1-yl)-3-(3,4-dimethoxyphenyl)prop-2-en-1-one (5b). Intermediate **3a** was treated with CH_3I **4b** to get target compound **5b**. Light yellow oil, 42.8% yield, 98.1% HPLC purity. ^{1}H NMR (400 MHz, $CDCl_3$) δ 7.59 (d, J = 15.6 Hz, 1H, CH = CH), 7.28 (t, J = 7.2 Hz, 2H, 2 × Ar-H), 7.20 (d, J = 7.2 Hz, 1H, Ar-H), 7.14 (d, J = 7.2 Hz, 2H, 2 × Ar-H), 7.09 (d, J = 6.4 Hz, 1H, Ar-H), 7.02 (d, J = 1.6 Hz, 1H, Ar-H), 6.85 (d, J = 8.0 Hz, 1H, Ar-H), 6.75 (d, J = 15.2 Hz, 1H, CH = CH), 4.71–4.69 (m, 1H, 1/2 $phCH_2$), 4.09–4.07 (m, 1H, 1/2 $phCH_2$), 3.91 (s, 3H, OCH_3), 3.90 (s, 3H, OCH_3), 3.04–3.02 (m, 1H, 1/2 NCH_2), 2.63–2.55 (m, 3H, 1/2 NCH_2 + NCH_2), 1.83–1.77 (m, 1H, CH), 1.74 (d, J = 13.6 Hz, 2H, CH_2), 1.28–1.17 (m, 2H, CH_2). ^{13}C NMR (101 MHz, $CDCl_3$) 165.6, 150.4, 149.1, 142.3, 140.0, 129.1, 128.5, 128.3, 126.1, 121.7, 115.4, 111.2, 109.9, 55.9, 46.2, 42.9, 38.4, 32.9, 31.8. HR-ESI-MS: Calcd. for $C_{23}H_{27}NO_3$ $[M + H]^+$: 366.2024, found: 366.2068.

4.1.2.3. (E)-3-(4-(benzyloxy)-3-methoxyphenyl)-1-(4-benzylpiperidin-1-yl)prop-2-en-1-one (5c). Intermediate **3a** was treated with benzyl bromide **4c** to get target compound **5c**. Light yellow oil, 49.7% yield, 97.4% HPLC purity. ^{1}H NMR (400 MHz, $CDCl_3$) δ 7.58 (d, J = 15.2 Hz, 1H, C = CH), 7.41 (d, J = 7.2 Hz, 2H, 2 × Ar–H), 7.36–7.31 (m, 2H, 2 × Ar–H), 7.29–7.23 (m, 4H, 4 × Ar–H), 7.19 (t, J = 7.2 Hz, 1H, Ar–H), 7.13–7.11 (m, 2H, 2 × Ar–H), 7.06–7.01 (m, 2H, 2 × Ar–H), 6.85–6.81 (m, 2H, 2 × Ar–H), 6.74 (d, J = 15.2 Hz, 1H, C = CH), 5.15 (s, 2H, OCH_2ph), 4.66–4.65 (m, 1H, 1/2 $phCH_2$), 4.07–4.05 (m, 1H, 1/2 $phCH_2$), 3.89 (s, 3H, OCH_3), 3.00–2.99 (m, 1H, 1/2 NCH_2), 2.55–2.48 (m, 3H, NCH_2 + 1/2 NCH_2), 1.81–1.77 (m, 1H, CH), 1.72 (d, J = 13.6 Hz, 2H, CH_2), 1.23–1.18 (m, 2H, CH_2). ^{13}C NMR (100 MHz, $CDCl_3$) δ 165.6, 149.7, 149.6, 142.3, 140.0, 139.9, 136.8, 132.7, 129.2, 129.1, 129.0, 128.9, 128.6, 128.4, 128.0, 127.3, 126.1, 121.5, 115.6, 113.7, 110.7, 70.9, 56.1, 46.6, 43.0, 41.3, 38.3, 32.2. HR-ESI-MS: Calcd. for $C_{29}H_{31}NO_3$ $[M + H]^+$: 442.2337, found: 442.2369.

4.1.2.4. (E)-1-(4-benzylpiperidin-1-yl)-3-(4-(cyclohexyloxy)-3-methoxyphenyl)prop-2-en-1-one (5d). Intermediate **3a** was treated with cyclohexyl bromide **4d** to get target compound **5d**. Light yellow oil, 60.2% yield, 97.3% HPLC purity. ^{1}H NMR (400 MHz, $CDCl_3$) δ 7.58 (d, J = 15.2 Hz, 1H, C = CH), 7.28 (t, J = 7.2 Hz, 2H, 2 × Ar–H), 7.20 (t, J = 7.2 Hz, 1H, Ar-H), 7.14 (d, J = 7.2 Hz, 2H, 2 × Ar–H), 7.07 (d, J = 6.4 Hz, 1H, Ar-H), 7.02 (s, 1H, Ar-H), 6.83 (d, J = 8.4 Hz, 1H, Ar-H), 6.73 (d, J = 15.2 Hz, 1H, CH = CH), 4.72–4.69 (m, 1H, 1/2 $phCH_2$), 4.10–4.06 (m, 1H, 1/2 $phCH_2$), 3.89 (s, 3H, OCH_3), 3.82 (d, J = 6.0 Hz, 2H, OCH_2), 3.04–3.03 (m, 1H, 1/2 NCH_2), 2.57–2.55 (m, 3H, NCH_2 + 1/2 NCH_2), 1.91–1.68 (m, 10H, 4 × CH_2 + 2 × CH), 1.31–1.18 (m, 4H, 4 × CH_2), 1.05–1.02 (m, 2H, CH_2). ^{13}C NMR (101 MHz, $CDCl_3$) δ 165.7, 150.4, 149.6, 142.5, 142.4, 140.0, 129.1, 128.3, 128.2, 126.1, 121.7, 115.1, 114.8, 112.7, 110.8, 74.5, 56.3, 43.0, 38.4, 37.4, 29.9, 26.5, 25.7. HR-ESI-MS: Calcd. for $C_{29}H_{37}NO_3$ $[M + H]^+$: 434.2650, found: 434.2691.

4.1.2.5. (E)-1-(3,4-dihydroisoquinolin-2(1H)-yl)-3-(3-methoxy-4-(prop-2-yn-1-yloxy)phenyl)prop-2-en-1-one (5e). Intermediate **3b** was treated with propargyl bromide **4a** to get target compound **5e**. Light yellow oil, 58.2% yield, 98.0% HPLC purity. ^{1}H NMR (400 MHz, $CDCl_3$) δ 7.66 (d, J = 15.2 Hz, 1H, C = CH), 7.19–7.12 (m, 5H, 5 × Ar-H), 7.07 (s, 1H, Ar-H), 7.02 (d, J = 8.4 Hz, 1H, Ar-H), 6.84 (d, J = 15.2 Hz, 1H, C = CH), 4.82 (s, 2H, $phCH_2$), 4.78 (d, J = 1.2 Hz, 2H, C≡$CHCH_2$), 3.91 (s, 3H, OCH_3), 3.87–3.85 (m, 2H, $phCH_2$), 2.95–3.88 (m, 2H, NCH_2), 2.55 (s, 1H, C≡CH). ^{13}C NMR (100 MHz, $CDCl_3$) 166.0, 149.7, 148.2, 142.6, 129.5, 128.3, 126.9, 126.6, 126.4, 121.3, 116.0, 115.8, 113.9, 110.7, 78.2, 76.2, 56.6, 56.0, 30.9, 29.7. HR-ESI-MS: Calcd. for $C_{22}H_{21}NO_3$ $[M + H]^+$: 348.1555, found: 348.1586.

4.1.2.6. (E)-1-(3,4-dihydroisoquinolin-2(1H)-yl)-3-(3,4-dimethoxyphenyl)prop-2-en-1-one (5f). Intermediate **3b** was treated with CH_3I **4b** to get target compound **5f**. Light yellow oil, 76.2% yield, 98.3% HPLC purity. ^{1}H NMR (400 MHz, $CDCl_3$) δ 7.67 (d, J = 15.2 Hz, 1H, C = CH), 7.19–7.12 (m, 5H, 5 × Ar-H), 7.06 (s, 1H, Ar-H), 6.86 (d, J = 8.0 Hz, 1H, Ar-H), 6.83 (d, J = 15.6 Hz, 1H, C = CH), 4.83 (s, 2H, $phCH_2$), 3.92 (s, 3H, OCH_3), 3.90 (s, 3H, OCH_3), 3.89–3.86 (m, 2H, NCH_2), 2.95–2.88 (m, 2H, NCH_2). ^{13}C NMR (100 MHz, $CDCl_3$) δ 166.1, 150.6, 149.1, 142.8, 128.3, 126.7, 126.6, 126.6, 121.9, 111.1, 110.0, 56.0, 44.8, 43.6, 29.7. HR-ESI-MS: Calcd. for $C_{20}H_{21}NO_3$ $[M + H]^+$: 324.1555, found: 324.1591.

4.1.2.7. (E)-3-(4-(benzyloxy)-3-methoxyphenyl)-1-(3,4-dihydroisoquinolin-2(1H)-yl)prop-2-en-1-one (5g). Intermediate **3b** was treated with benzyl bromide **4c** to get target compound **5g**. Light yellow oil, 50.9% yield, 97.8% HPLC purity. ^{1}H NMR (400 MHz, $CDCl_3$) δ 7.66 (d, J = 15.2 Hz, 1H, C = CH), 7.34 (d, J = 7.2 Hz, 2H, 2 × Ar-H), 7.28 (t, J = 7.6 Hz, 2H, 2 × Ar-H), 7.22 (d, J = 7.2 Hz, 1H, Ar-H), 7.14–7.00 (m, 4H, 4 × Ar-H), 6.99–6.96 (m, 1H, Ar-H), 6.78 (d, J = 8.8 Hz, 1H, Ar-H), 6.72 (d, J = 15.2 Hz, 1H, Ar-H), 5.09 (s, 2H, $phCH_2$), 4.74 (s, 2H, $phCH_2$), 3.84 (s, 3H, OCH_3), 3.79–3.75 (m, 2H,

NCH_2), 2.86–2.82 (m, 2H, NCH_2). HR-ESI-MS: Calcd. for $C_{26}H_{25}NO_3$ $[M+H]^+$: 400.1868, found: 400.1872.

4.1.2.8. (E)-3-(4-(cyclohexyloxy)-3-methoxyphenyl)-1-(3,4-dihydroisoquinolin-2(1H)-yl)prop-2-en-1-one (5h). Intermediate **3b** was treated with cyclohexyl bromide **4d** to get target compound **5h**. Light yellow oil, 39.2% yield, 97.7% HPLC purity. ^{1}H NMR (400 MHz, $CDCl_3$) δ 7.59 (d, $J=15.6$ Hz, 1H, C = CH), 7.14–7.10 (m, 4H, 4 × Ar-H), 7.03 (d, $J=8.4$ Hz, 1H, Ar-H), 6.99 (d, $J=2.0$ Hz, 1H, Ar-H), 6.82 (d, $J=8.0$ Hz, 1H, Ar-H), 6.73 (d, $J=15.6$ Hz, 1H, C = CH), 4.77 (s, 2H, $phCH_2$), 4.19–4.16 (m, 1H, CH), 3.85–3.79 (m, 5H, OCH_3 + $phCH_2$), 2.89–2.86 (m, 2H, NCH_2), 1.99–1.95 (m, 2H, CH_2), 1.79–1.72 (m, 2H, CH_2), 1.55–1.47 (m, 4H, 4 × CH_2), 1.27–1.22 (m, 2H, CH_2). HR-ESI-MS: Calcd. for $C_{25}H_{29}NO_3$ $[M+H]^+$: 392.2181, found: 392.2216.

4.1.2.9. (E)-1-(4-benzylpiperazin-1-yl)-3-(3,4-dimethoxyphenyl)prop-2-en-1-one (5i). Intermediate **3c** was treated with CH_3I **4b** to get target compound **5i**. Light yellow oil, 53.9% yield, 98.3% HPLC purity. ^{1}H NMR (400 MHz, $CDCl_3$) δ 7.61 (d, $J=15.2$ Hz, 1H, CH = CH), 7.33–7.31 (m, 4H, 4 × Ar-H), 7.29–7.26 (m, 1H, Ar-H), 7.10 (dd, J_1 = 6.8 Hz, J_2 = 1.6 Hz, 1H, Ar-H), 7.02 (d, $J=1.6$ Hz, 1H, Ar-H), 6.85 (d, $J=8.4$ Hz, 1H, Ar-H), 6.72 (d, $J=15.2$ Hz, 1H, CH = CH), 3.91 (s, 3H, OCH_3), 3.90 (s, 3H, OCH_3), 3.75–3.72 (m, 2H, NCH_2), 3.67–3.64 (m, 2H, NCH_2), 3.54 (s, 2H, $phCH_2$), 2.49 (t, $J=4.8$ Hz, 4H, 2 × NCH_2). ^{13}C NMR (100 MHz, $CDCl_3$) 165.6, 150.5, 149.1, 142.7, 137.6, 129.2, 128.3, 127.3, 121.8, 114.9, 111.1, 109.9, 62.9, 55.9, 52.8. HR-ESI-MS: Calcd. for $C_{22}H_{26}N_2O_3$ $[M+H]^+$: 367.1977, found: 367.2006.

4.2. Biological activity experiments

4.2.1. Recombinant human MAO-A and MAO-B inhibition studies

Recombinant human MAO-A and MAO-B were purchased from Sigma-Aldrich and stored at −80 °C. The detailed procedure could reference the previous work[18,21]. Briefly, tested compounds were prepared in DMSO (2.5 mM) and diluted with potassium phosphate buffer (100 mM, pH 7.40, containing KCl 20.2 mM) to a final volume of 500 μL containing various concentrations of test compounds (0–100 μM) and kynuramine (45 μM for MAO-A and 30 μM for MAO-B). The reactions were initiated by the addition of the enzyme (7.5 μg/mL) and then incubated for 30 min at 37. Then 400 μL NaOH (2 N) and 1000 μL water were added to terminate the enzymatic reactions and the mixtures were centrifuged at 16,000 g for 10 min. The concentrations of the generated 4-hydroxyquinoline were determined by measuring the fluorescence of the supernatant on a Varioskan Flash Multimode Reader (PerkinElmer) with excitation and emission wavelengths at 310 and 400 nm, respectively. IC_{50} values were calculated from sigmoidal dose-response curves (graphs of the initial rate of kynuramine oxidation versus the logarithm of inhibitor concentration). Each sigmoidal curve was constructed from six different compound concentrations spanning at least three orders of magnitude. Data analyses were carried out with GraphRad Prism 5 employing the one-site competition model. IC_{50} values were determined in triplicate and expressed as mean ± *SD*.

4.2.2. Molecular modelling docking[18,21]

The crystal structure of human MAO-B in complex with the selective inhibitor 7–(3-chlorobenzyloxy)-4-carboxaldehyde-coumarin (PDB code: 2V60) was obtained from the Protein Data Bank after eliminating the original inhibitors and water molecules. The 3 D Structure of **5a** was built and performed geometry optimisation by molecular mechanics. After the addition of Gasteiger charges, removal of hydrogen atoms, the addition of the atomic charges to skeleton atoms, and the assignment of proper atomic types, the further preparation of the inhibitor was accomplished. Docking studies were performed using the AUTODOCK 4.2.6 program. By using Autodock Tools (ADT: version 1.5.6), polar hydrogen atoms were added to amino acid residues, and Gasteiger charges were assigned to all atoms of the enzyme. The resulting enzyme structure was used as an input for the AUTOGRID program. AUTOGRID performed pre-calculated atomic affinity grid maps for each atom type in the ligand. The centre of the grid box was placed with coordinated $x=14.846$, $y=128.673$, $z=24.971$. The dimensions of the active site box were set at 50 × 50 × 50 Å. Flexible ligand docking was performed for the compound. Each docked system was performed by 100 runs of the AUTODOCK search by the Lamarchian genetic algorithm (LGA). A cluster analysis was performed on the docking results using a root mean square (RMS) tolerance of 1.0 and the lowest energy conformation of the highest populated cluster was selected for analysis. Graphic manipulations and visualisations were done by Autodock Tools or Discovery Studio 2.1 software.

4.2.3. Effects on self-mediated A$\beta_{1\text{-}42}$ aggregation

A$\beta_{1\text{-}42}$ was purchased from ChinaPeptides Co., Ltd. The experiments include inhibition experiments and disaggregation experiments. The detailed procedure referenced our previous work[25]. Briefly, the A$\beta_{1\text{-}42}$ samples were incubated in 50 mM phosphate buffer solution (pH 7.4) at 37 °C for 24 h (final Aβ concentration of 25 μM) with or without the tested compounds (25 μM, final concentration). After incubation, 160 μL of thioflavin T (5 μM in 50 mM glycine-NaOH buffer pH 8.0) was added. Each assay was run in triplicate. Fluorescence was measured with excitation and emission wavelengths at 446 and 490 nm, respectively. The fluorescence intensities were calculated by the expression $(1\text{-}IF_i/IF_c) \times 100$, in which IF_i and IF_c are the fluorescence intensities obtained for A$\beta_{1\text{-}42}$ in the presence and absence of inhibitors after subtracting the background, respectively.

For the disaggregation of self-induced Aβ fibrils experiment, the A$\beta_{1\text{-}42}$ stock solution was diluted in phosphate buffer solution (pH 7.4). The mixture of the A$\beta_{1\text{-}42}$ (20 μL, 25 μM, final concentration) was incubated at 37 °C for 24 h. The tested compounds (20 μL, 25 μM, final concentration) were then added and incubated at 37 °C for another 24 h. After incubation, 160 μL of 5 μM thioflavin T in 50 mM glycine-NaOH buffer (pH 8.5) was added. Each assay was run in triplicate. The detection method was the same as described above.

4.2.4. Transmission electron microscopy assay

Ten microlitres of the samples, obtained from the ThT assay, were added into a carbon-coated copper/rhodium grid for 2 min. Each grid was incubated with uranyl acetate (1% w/v ddH_2O). Upon removal of excess uranyl acetate, the grids were dried for 15 min at room temperature. Images from each sample were taken on a Field Emission Transmission Electron Microscope (JEM-2100F).

4.2.5. Blood − brain barrier permeation assay

The BBB penetration *in vitro* of compounds was tested through a PAMPA assay. The detailed procedure referenced our previous paper[25]. Briefly, the commercial drugs were purchased from Sigma

and Alfa Aesar. Porcine brain lipid (PBL) was purchased from Avanti Polar Lipids. Both the donor microplate (PVDF membrane, pore size 0.45 mm) and acceptor microplate were obtained from Millipore. The 96-well UV plate (COSTAR) was from Corning Incorporated. The acceptor 96-well microplate was filled with 350 μL of PBS/EtOH (70:30), and the filter membrane was impregnated with 4 μL of PBL in dodecane (20 mg/mL). Compounds were dissolved in DMSO at 5 mg/mL and diluted 50-fold in PBS/EtOH (70:30) to a final concentration of 100 μg/mL. Then 200 μL of the solution was added to the donor wells. The acceptor filter plate was carefully placed on the donor plate to form a sandwich, which was left undisturbed for 18 h at 25 °C. After incubation, the donor plate was carefully removed, and the concentration of compounds in the acceptor wells was determined using the Varioskan Flash Multimode Reader. Every sample was analysed at ten wavelengths in four wells and in at least three independent runs. Pe was calculated using the following expression: $P_e = \{-V_d V_a/[(V_d + V_a)At]\}\ln(1 - \text{drug}_{\text{acceptor}}/\text{drug}_{\text{equilibrium}})$, where V_d is the volume of donor well, V_a is the volume in the acceptor well, A is the filter area, t is the permeation time, drug acceptor is the absorbance obtained in the acceptor well, and drug equilibrium is the theoretical equilibrium absorbance. The results are given as the mean ± standard deviation. In the experiment, 11 quality control standards of known BBB permeability were included to validate the analysis set. A plot of the experimental data versus literature values gave a strong linear correlation, $P_e(\text{exp}) = 0.9163P_e(\text{bibl.}) - 0.2247$ ($R^2 = 0.9558$). From this equation and the limit established by Di et al. (P_e (bibl.) $= 4.0 \times 10^{-6}$ cm/s) for blood – brain barrier permeation, we concluded that compounds with a permeability $>3.44 \times 10^{-6}$ cm/s could cross the blood – brain barrier.

4.2.6. In vivo *PET-CT imaging with [^{11}C]5f in mice*

All animal imaging studies were carried out at Massachusetts General Hospital (PHS Assurance of Compliance No. A3596–01). All mice were socially housed in cages appropriate for the physical and behavioural health of the individual animal and were given unlimited access to food and water, with additional nutritional supplements provided as prescribed by the attending veterinary staff.

4.2.6.1. Radiosynthesis of [11C]5f. The radiosynthesis of [^{11}C]**5f** referred to our previous work. Briefly, [^{11}C]CH_3I was trapped in the solution of precursor **3b** (1.0 mg) and NaOH (5.0 mg) in anhydrous DMF (0.3 ml). The mixture was injected into the semi-preparative reversed-phase HPLC (Agilent Eclipse XDB–C18, 5 μm, 9.4 × 250 mm, eluting with a mobile phase of 38% H_2O + 0.1% TFA/62% CH_3CN, at the flow rate of 5.0 ml/min). The product-contain collection was reformulated by solid-phase exchange (SPE) C-18 cartridges. The process of [^{11}C]**5f** preparation was accomplished in 30–40 min after the end of bombardment (EOB), with an overall non-decay corrected radiochemical yields (12–15%, $n = 3$) at the end of synthesis (EOS) and specific activity of 83.2 GBq/μmol (EOB).

4.2.6.2. Mice PET/CT acquisition and post-processing. Rodent PET/CT imaging studies were conducted in male C57BL/6 mice in groups. Each test group contained 4 mice, anaesthetised with inhalational isoflurane (Patterson Vet Supply, Inc., Greeley, CO, USA) at 2% in a carrier of 2 L/min medial oxygen, and maintained at 1.2% isoflurane for the duration of the imaging scanning. The mice were arranged in a Triumph Trimodality PET/CT/SPECT scanner (Gamma Medica, Northridge, CA, USA). Mice were injected with standard reference or vehicle *via* a lateral tail vein catheterisation 5-min before the start of PET acquisition for the blocking study. Dynamic PET acquisition lasted for 60 min followed by computed tomography (CT) for anatomic co-registration. Reconstructed PET images were exported from the scanner in DICOM format along with an anatomic CT for analysis. Initial data were imported and analysed using AMIDE software[31] (an open-source software, Los Angeles, CA, USA) and PMOD (PMOD 4.01, PMOD Technologies Ltd., Zurich, Switzerland).

4.2.6.3. Mice PET–CT image analysis. Volumes of interest (VOIs) were generated manually in the forms of spheres under the guidance of high–resolution CT structural images and summed PET data, with a radius no <1 mm to minimise partial volume effects. Time–activity curves (TACs) were exported as decay–corrected activity per unit volume. The TACs were expressed as percent injected dose per unit volume for analysis.

Disclosure statement

The authors declare no competing financial interest.

Funding

This work was financially supported by the National-Local Joint Engineering Research Center for Innovative & Generic Chemical Drug, and Guizhou High-level Innovative Talents Supporting Program (2016–4015); The State Key Laboratory of Functions and Applications of Medicinal Plants, Guizhou Medical University (Grant number FAMP202107K); Guizhou Science and Technology Platform Talents (QKHRCPT[2019]5627), and the Special Project of Nanyang Normal University (2022QN003).

References

1. Barnett R. Alzheimer's disease. Lancet 2019;393:1589.
2. Citron M. Alzheimer's disease: strategies for disease modification. Nat Rev Drug Discov 2010;9:387–98.
3. Viña J, Sanz-Ros J. Alzheimer's disease: only prevention makes sense. Eur J Clin Invest 2018;48:e13005.
4. Jagust W. Imaging the evolution and pathophysiology of Alzheimer disease. Nat Rev Neurosci 2018;19:687–700.
5. Schedin-Weiss S, Inoue M, Hromadkova L, et al. Monoamine oxidase B is elevated in Alzheimer disease neurons, is associated with γ-secretase and regulates neuronal amyloid β-peptide levels. Alzheimers Res Ther 2017;9:57.
6. Available from: https://www.alzforum.org/therapeutics/rasagiline
7. Calsolaro V, Edison P. Neuroinflammation in Alzheimer's disease: current evidence and future directions. Alzheimers Dement 2016;12:719–32.
8. Tamagno E, Guglielmotto M, Vasciaveo V, Tabaton M. Oxidative stress and beta amyloid in Alzheimer's disease. Which comes first: the chicken or the egg? Antioxidants 2021;10:1479.
9. de Freitas Silva M, Dias KST, Gontijo VS Jr., et al. Multi-target directed drugs as a modern approach for drug design towards Alzheimer's disease: an update. Curr Med Chem 2018;25:3491–525.

10. Cavalli A, Bolognesi ML, Minarini A, et al. Multi-target-directed ligands to combat neurodegenerative diseases. J Med Chem 2008;51:347–72.
11. Zhang P, Xu S, Zhu Z, Xu J. Multi-target design strategies for the improved treatment of Alzheimer's disease. Eur J Med Chem 2019;176:228–47.
12. Available from: http://integrity.thomson-pharma.com
13. Sgarbossa A, Giacomazza D, di Carlo M. Ferulic acid: a hope for Alzheimer's disease therapy from plants. Nutrients 2015; 7:5764–82.
14. Nabavi SF, Devi KP, Malar DS, et al. Ferulic acid and Alzheimer's disease: promises and pitfalls . Mini Rev Med Chem 2015;15:776–88.
15. Legoabe LJ, Petzer A, Petzer JP. 2-acetylphenol analogs as potent reversible monoamine oxidase inhibitors. Drug Des Devel Ther 2015;9:3635–44.
16. Li T, Pan W, Wang K, et al. Novel ferulic acid-donepezil hybrids as multifunctional agents for the treatment of Alzheimer's disease with butyrylcholinesterase, amyloid-β, antioxidant and neuroprotective properties. Lett Drug Des Discov 2017;14:918–29.
17. Bai P, Wang K, Zhang P, et al. Development of chalcone-O-alkylamine derivatives as multifunctional agents against Alzheimer's disease. Eur J Med Chem 2019;183:111737.
18. Sang Z, Wang K, Zhang P, et al. Design, synthesis, *in-silico* and biological evaluation of novel chalcone derivatives as multi-function agents for the treatment of Alzheimer's disease. Eur J Med Chem 2019;180:238–52.
19. Knez D, Colettis N, Iacovino LG, et al. Stereoselective activity of 1-propargyl-4-styrylpiperidine-like analogues that can discriminate between monoamine oxidase isoforms A and B. J Med Chem 2020;63:1361–87.
20. Wang XB, Yin FC, Huang M, et al. Chromone and donepezil hybrids as new multipotent cholinesterase and monoamine oxidase inhibitors for the potential treatment of Alzheimer's disease. RSC Med Chem 2020;11:225–33.
21. Tian C, Qiang X, Song Q, et al. Flurbiprofen-chalcone hybrid Mannich base derivatives as balanced multifunctional agents against Alzheimer's disease: design, synthesis and biological evaluation. Bioorg Chem 2020;94:103477.
22. Sang Z, Wang K, Shi J, et al. The development of advanced structural framework as multi-target-directed ligands for the treatment of Alzheimer's disease. Eur J Med Chem 2020;192: 112180.
23. Sang Z, Wang K, Shi J, et al. Apigenin-rivastigmine hybrids as multi-target-directed ligands for the treatment of Alzheimer's disease. Eur J Med Chem 2020;187:111958.
24. Cao Z, Yang J, Xu R, et al. Design, synthesis and evaluation of 4′-OH-flurbiprofen-chalcone hybrids as potential multi-functional agents for Alzheimer's disease treatment. Bioorg Med Chem 2018;26:1102–15.
25. Sang Z, Wang K, Bai P, et al. Design, synthesis and biological evaluation of novel O-carbamoyl ferulamide derivatives as multi-target-directed ligands for the treatment of Alzheimer's disease. Eur J Med Chem 2020;194:112265.
26. Tong Y, Bai L, Gong R, et al. Shikonin protects PC12 cells against β-amyloid peptide-induced cell injury through anti-oxidant and antiapoptotic activities. Sci Rep 2018;8:26.
27. Di L, Kerns EH, Fan K, et al. High throughput artificial membrane permeability assay for blood-brain barrier. Eur J Med Chem 2003;38:223–32.
28. Available from: https://www.molinspiration.com/cgi-bin/properties
29. Wang C, Schroeder FA, Hooker JM. Development of new positron emission tomography radiotracer for BET imaging. ACS Chem Neurosci 2017;8:17–21.
30. Wang C, Schroeder FA, Wey HY, et al. *In vivo* imaging of histone deacetylases (HDACs) in the central nervous system and major peripheral organs. J Med Chem 2014;57: 7999–8009.
31. Loening AM, Gambhir SS. AMIDE: a free software tool for multimodality medical image analysis. Mol Imaging 2003;2: 131–7.